remote sensing

MDPI

Article

How Well Does the 'Small Fire Boost' Methodology Used within the GFED4.1s Fire Emissions Database Represent the Timing, Location and Magnitude of Agricultural Burning?

Tianran Zhang [1,2,*], Martin J. Wooster [1,2], Mark C. de Jong [1,2] and Weidong Xu [1,2]

[1] Department of Geography, King's College London, Strand, London WC2R 2LS, UK; martin.wooster@kcl.ac.uk (M.J.W.); mark.dejong@kcl.ac.uk (M.C.d.J.); weidong.xu@kcl.ac.uk (W.X.)
[2] NERC National Centre for Earth Observation (NCEO), King's College London, London WC2R 2LS, UK
* Correspondence: tianran.zhang@kcl.ac.uk

Received: 17 April 2018; Accepted: 18 May 2018; Published: 25 May 2018

Abstract: The Global Fire Emissions Database (GFED)—currently by far the most widely used global fire emissions inventory—is primarily driven by the 500 m MODIS MCD64A1 burned area (BA) product. This product is unable to detect many smaller fires, and the new v4.1s of GFED addresses this deficiency by using a 'small fire boost' (SFB) methodology that estimates the 'small fire' burned area from MODIS active fire (AF) detections. We evaluate the performance of this approach in two globally significant agricultural burning regions dominated by small fires, eastern China and north-western India. We find the GFED4.1s SFB can affect the burned area and fire emissions data reported by GFED very significantly, and the approach shows some potential for reducing low biases in GFED's fire emissions estimates of agricultural burning regions. However, it also introduces several significant errors. In north-western India, the SFB slightly improves the temporal distribution of agricultural burning, but the magnitude of the additional burned area added by the SFB is far too low. In eastern China, the SFB appears to have some positive effects on the magnitude of agricultural burning reported in June and October, but significant errors are introduced in the summer months via false alarms in the MODIS AF product. This results in a completely inaccurate 'August' burning period in GFED4.1s, where false fires are erroneously stated to be responsible for roughly the same amount of dry matter fuel consumption as fires in June and October. Even without the SFB, we also find problems with some of the burns detected by the MCD64A1 burned area product in these agricultural regions. Overall, we conclude that the SFB methodology requires further optimisation and that the efficacy of GFED4.1s' 'boosted' BA and resulting fire emissions estimates require careful consideration by users focusing in areas where small fires dominate.

Keywords: biomass burning; burned area; active fire; MODIS; VIIRS; Sentinel-2; Landsat

1. Introduction

The Global Fire Emissions Database (GFED) is currently the most widely used global fire emissions inventory. It is based on the Seiler and Crutzen [1] approach that multiplies mapped burned area (BA) by modelled fuel consumptions and species-specific gas and aerosol emission factors to estimate fire emissions at a 0.25° spatial resolution [2]. The BA maps used by GFED are provided by NASA's 500-m spatial resolution MODIS BA product (MCD64A1), which classifies pixels as burned using a spectral reflectance-based change detection technique [3]. The BA signature of landscape fires typically lasts for several days to several months post-fire (depending on biome), making these BA maps somewhat immune to cloud-cover and satellite observation gaps [3]. This contrasts with the

active fire (AF) detection approach which can identify fires only if they are burning and the area is cloud-free at the time of the satellite observation [4,5]. However, whilst BA products typically require a substantial part (approximately $\geq$ 20%) of a pixel to be burned before a BA algorithm can identify it as 'fire-affected' [5,6], active fires filling only 0.01–0.1% of a pixel are relatively easily identified due to their high thermal contrast relative to the surrounding ambient background [7,8]. BA and AF products are therefore highly complementary sources of fire information [9], though traditionally GFED has focused on the use of BA data, apart from for the early years of the inventory (late 1990's and early 2000's) when the MODIS BA product is unavailable [10]. Whilst GFED has been evaluated many times and shown to provide high quality data for the main global regions where 'large-fire' dominated biomass burning occurs [2,3], its performance in regions dominated by 'small fires' has remains questionable. In particular, Randerson et al. [11] highlighted that the MCD64A1 BA product typically fails to detect many of the burns in 'small fire dominated' areas, because the changes in landscape spectral reflectance are often not significant enough to be confidently identified by the 500-m MCD64A1 BA algorithm. A 'small fire boost' (SFB) strategy was therefore proposed by [11] to counteract this underestimation. The strategy was based on the use of MODIS AF detections and surface spectral reflectance change analysis, with the aim of estimating the BA remaining undetected by the MODIS MCD64A1 product, and thus 'boosting' the MCD64A1 burned area through this additional measure. The SFB was shown to have by far the greatest impact in agricultural regions of certain developing nations, where recurrent crop residue burning has major implications for regional air quality [12–16]. In such regions, Randerson et al. [11] indicated that the SFB strategy increased the BA detected by MCD64A1 by 80–90%, and based on this demonstration, an adaptation of the approach was introduced into the most recent version of GFED (GFED4.1s; [10]). Compared to the forerunner GFED4 inventory, the addition of the SFB methodology to GFED's calculations resulted in similarly dramatic increases in reported BA in certain agricultural regions. Here we investigate the efficacy of these upward adjustments in burned area, and specifically their impact on the timing, location and magnitude of fire activity metrics provided by GFED4.1s in small fire dominated regions. We explore the veracity of the additionally 'boosted' BA measures though comparison with independent data sources, focusing on two regions dominated by agricultural burning—eastern China and the Punjab region of north-western India. For the years examined here, in eastern China (2015–2016) GFED4.1s shows a burned area 665% higher than that reported by GFED4, but in the Punjab region (2016) GFED4.1s is only 26% higher. We therefore also examine why some agricultural regions show far greater impacts from the GFED4.1s BA 'boost' than others.

2. Datasets, Study Areas and Data Processing

2.1. Datasets

The study makes use of several multi-sensor datasets (summarised in Table 1) for various periods between 2015 and 2016. The GFED4 and GFED4.1s databases were obtained from https://www.geo.vu.nl/~gwerf/GFED/GFED4/, and the MODIS MCD64A1 monthly BA (Collection 6) from ftp://fuoco.geog.umd.edu (all at 0.25° grid cell resolution). The original MODIS 500 m MCD64A1 BA and 1-km MODIS MCD14 AF products were downloaded from https://earthexplorer.usgs.gov/. We used the VIIRS-IM AF and FRP product described in Zhang et al. [17] as one of our independent data sources. This active fire product blends the advantages of VIIRS' 375 m I-Band for detecting 'small' active fires, with the 750 m spatial resolution VIIRS M-Band's ability to retrieve fire radiative power (FRP) over large and intensely burning fires without saturation. Due to the VIIRS I-Band's 10× smaller pixel area, this AF product has been shown to detect many more of the small agricultural fires (and thus, on average, ~4 times more FRP) in eastern China compared to near simultaneously collected MODIS MCD14 data (which is based on MODIS' 1 km pixels, which also increase considerably in size away from nadir) [17]. To provide more spatially detailed information over our study areas we

also used Level 1b imagery from Landsat 7 and 8 and Sentinel-2 MSI (Multispectral Instrument), obtained from https://glovis.usgs.gov/.

Table 1. Summary of the multi-sensor datasets used herein.

Dataset	System	Resolution
GFED4 Burned Area GFED4.1s Burned Area	MODIS, ATSR, VIIRS	0.25°
MCD64A1 Burned Area	MODIS	500 m
MCD14 Active Fire	MODIS	1 km
VIIRS Regional Active Fire	VIIRS	375 m
Landsat Level 1B product	Landsat 7/8	30 m
Sentinel-2 Level 1B product	Sentinel-2 MSI	10, 20, 60 m

2.2. Study Areas

The area of eastern China studied here spans 111–123° E and 27–41° N, covering 1.7 million km^2 (Figure 1). It is responsible for an estimated 25% of China's crop production (~51% of the national rice yield; [18]), and is home to around one third of the Chinese population. This area sees widespread agricultural burning of wheat, rice and other agricultural residues, and is believed to be responsible for more than 50% of China's total biomass burning emissions [13,19]. However, typical agricultural field sizes are small, reportedly a mean of around 700 m^2, and thus equivalent to only ~0.25% of the area of a 500 m MODIS pixel [18]. For this reason, many such fields would need to be burned within a single MODIS 500 m pixel to result in a successful BA detection via spectral reflectance change detection methods, and this is the reason for the very significant underestimation of BA typically reported in such regions by the MCD64A1 BA product [11]. Nevertheless, satellite data are effective enough to show recurrent burning across this eastern China region occurs around June and October every year [17].

The north-western India study area surrounding the Punjab region (73–78° E, 27–33° N; Figure 2) covers 0.3 million km^2. This area encompasses the main agricultural residue burning region of India [20], with state-wide inventories reporting that ~16% of the total crop residue production of 620 T_g is burned in fields [21], primarily between October to November every year, but with a secondary burning peak in May [20].

2.3. Landsat and Sentinel-2 Data Processing

For comparison to the coarser spatial resolution BA data derived from MODIS at 500 m pixel size (and presented in the GFED4.1s inventory at 0.25°), Sentinel-2 and Landsat ETM+ imagery were used to map burned areas at 100-m spatial resolution, based on the differencing of pre- and post-fire normalised burn ratio measures (dNBR) as developed by [22]:

$$\mathrm{dNBR} = \left[\frac{\rho_{SWIR} - \rho_{NIR}}{\rho_{SWIR} + \rho_{NIR}}\right]_{pre-fire} - \left[\frac{\rho_{SWIR} - \rho_{NIR}}{\rho_{SWIR} + \rho_{NIR}}\right]_{post-fire}$$

Here ρ_{SWIR} and ρ_{NIR} refer to the top-of-atmosphere (TOA) reflectance recorded in the short-wave infrared and near infrared bands (Band 7 and 5 for Landsat 8 and Band 12 and 8A for Sentinel-2). The combined use of these two sensors in a similar way has previously been reported by [23].

Following [22], a simple dNBR threshold was used to differentiate unburned (dNBR < 0.27) and burned pixels (dNBR $\geq$ 0.27), and the summed area of the latter used to calculate total BA for the scene. Because the high spatial resolution of the input data is of a similar size to the agricultural fields, it is expected that this dNBR-based metric provides reasonable mapping of BA in this small-fire dominated, agricultural environment [22].

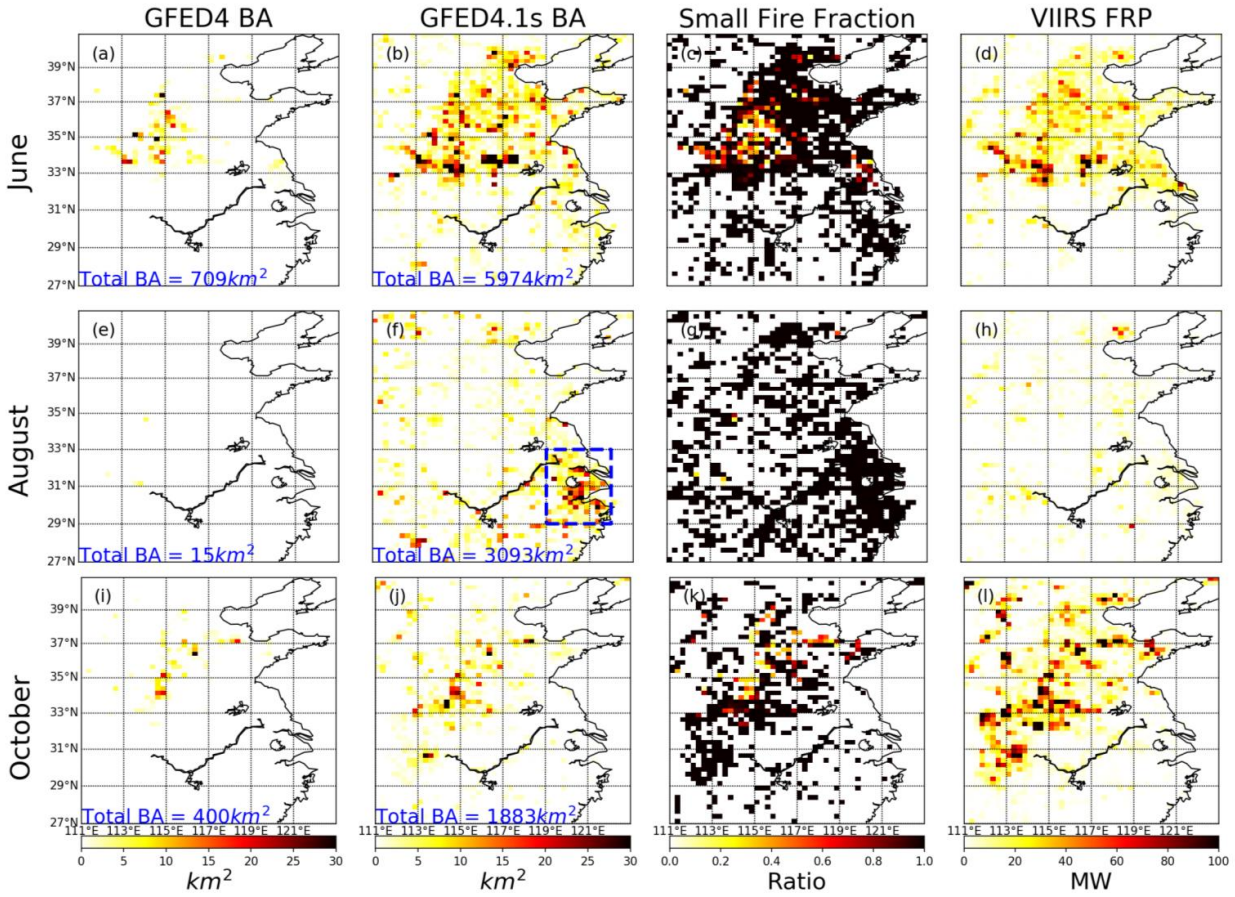

Figure 1. Spatial mapping (0.25°) of the fire affected regions for 2015 in eastern China in June (**a**–**d**), August (**e**–**h**) and October (**i**–**l**). (1st column) burned area (BA) reported by GFED4, which uses the MODIS MCD64A1 BA product as its BA metric for all years after the early 2000's. (2nd column) BA reported by the most recent GFED4.1s inventory, which increases the basic MCD64A1 measured BA via an adaptation of the 'small fire boosting' approach developed by [11] (which is primarily driven by MODIS AF detections). (3rd column) Fraction of BA reported by GFED4.1s that comes from the SFB methodology of [11], and (4th column) the fire radiative power (FRP) reported in the same area by the VIIRS-IM product of Zhang et al. [17] that is sensitive to both small and large fires. June and October are the periods of most intensive agricultural burning in this region of eastern China [17,21], which makes the 'strongly boosted' BA seen in August in GFED4.1s (highlighted with the blue dashed rectangle in (**f**)) seem potentially erroneous, and at odds with a lack of fire activity reported by the VIIRS-IM product for the same month (**h**).

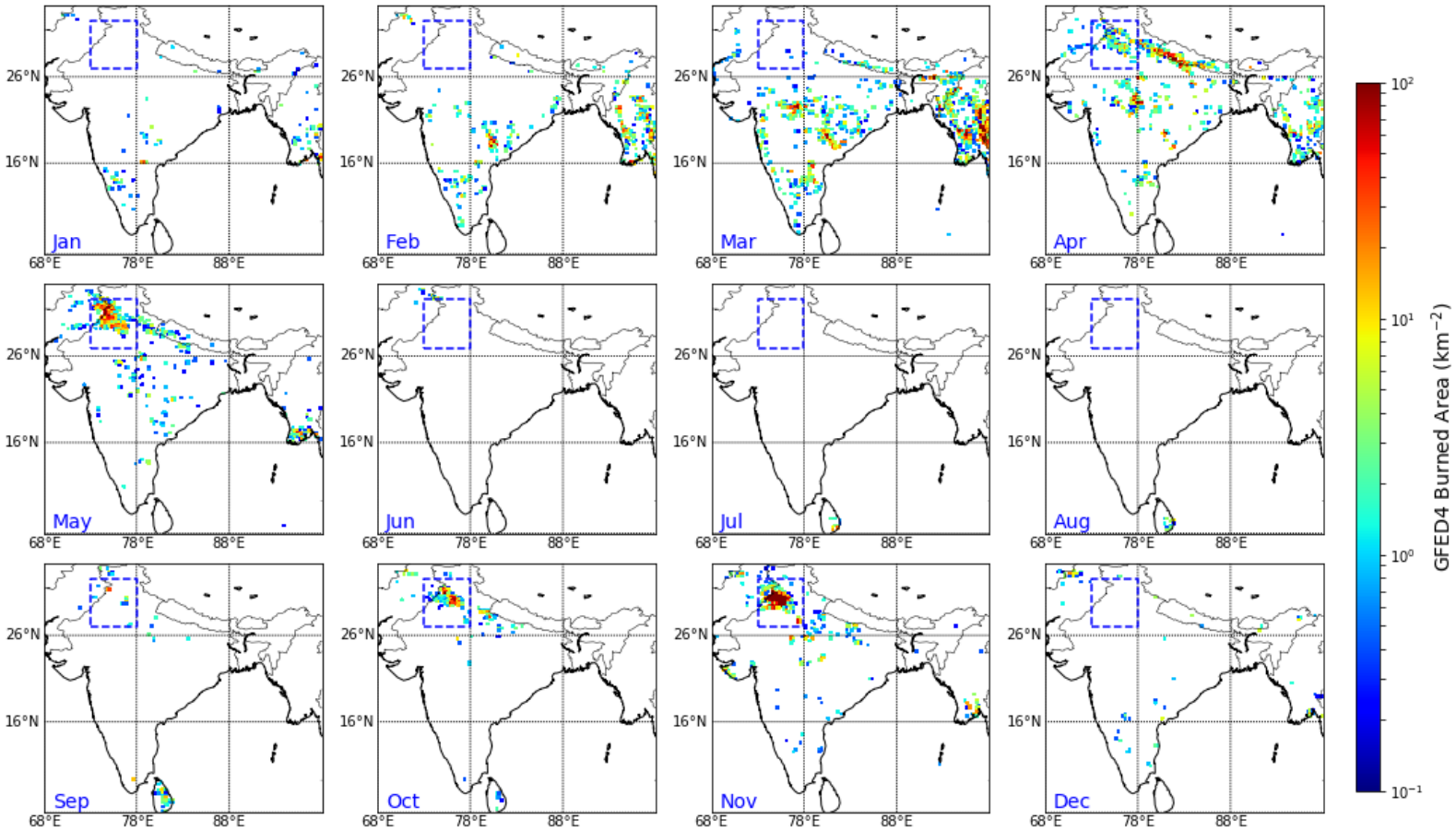

Figure 2. Monthly burned area (0.25°) reported for 2016 across India by the MCD64A1 product, as derived from 500 m MODIS observations using the algorithm of [4] and reported by GFED4. In Punjab, north-western India (highlighted by the blue rectangle) fire shows a strong seasonal pattern, with activity occurring primarily in May and then again (stronger) in October and November. These periods are associated primarily with agricultural fires, with wheat stubble primarily burned in May and rice straw in October–November.

3. Evaluation of GFED4.1s 'Small Fire Boosting'

3.1. Eastern China

Figure 1 illustrates the degree of adjustment made to eastern China's reported BA within GFED4.1s using the SFB approach for the key months of June, August and October 2015. This period encompasses the times within which the vast majority of burning occurs in this region [24]. Compared to GFED4, GFED4.1s identifies far more BA, both by reporting a generally higher BA within 0.25° cells where both inventories identify the presence of fire, and by reporting additional BA in cells where GFED4s reports no fire at all. The BA reported by GFED4.1s for June and October 2015 is 4× higher than that reported by GFED4, and the increased spatial extent of the fire affected region reported by GFED4.1s (Figure 1b,j) seems to agree far more with the FRP maps derived from the VIIRS-IM AF product developed by [17] and shown for the same months in Figure 1d,i. This indicates that the GFED4.1s SFB is very likely to be improving the agricultural fire emissions estimates of these months over those of the forerunner GFED4 version, which clearly fails to identify much of the burning in this region during June and October (Figure 1a,i). However, a very high BA (3093 km^2) is also reported by GFED4.1s in August, with most located between 29–33° N and 119–122° (the area identified by the blue rectangle in Figure 1f). August is not a month known to be associated with agricultural burning in this area of eastern China, and this is confirmed by the lack of any significant fire activity in both the original GFED4 inventory (Figure 1e) and in the 'small fire sensitive' VIIRS FRP record (Figure 1h). Thus, whilst the SFB methodology included in GFED4.1s appears to have delivered some potential benefits during the months of June and October when many fires are certainly present in this landscape, its use in August has led to a new and very significant area of burning being reported that is likely incorrect.

Examination of Sentinel-2 and Landsat imagery for the suspicious area of GFED4.1s August burning highlighted in Figure 1f shows that, in fact, this area is not agricultural at all but is a high density urban area with little agricultural land, which is very unlikely to experience significant landscape burning. During development of the VIIRS-IM AF detection algorithm, large numbers of 'false alarm' VIIRS AF detections were initially found in this area of eastern China, caused by industrial activity and buildings whose rooftops are significantly more reflective and/or warmer than their surroundings [17]. Temporal filtering of these detections, along with landcover-based urban area masking, was used to screen out these false alarms in the final VIIRS-IM AF product [17]. However, no such filtering is applied within the MODIS MCD14 AF products, which are used to generate the SFB used in GFED4.1s. Therefore, it is likely that AF 'false alarms' present in the MODIS MCD14 products of this area are causing incorrectly boosted BA in GFED4.1s during August 2015.

The 10 m spatial resolution Sentinel-2 MSI true colour composite imagery provides high enough spatial detail to observe individual agricultural fields, and to examine the efficacy of the MODIS AF detections, the MCD14 dataset (observed during August 2016) was overlain on the Sentinel-2 MSI imagery (Figure 3). This confirmed that most MODIS AF detections were located in non-agricultural areas, and so are very likely false alarms caused by the same types of urban features that initially resulted in erroneous AF detections in the unmasked VIIRS-IM AF product developed by [17]. In the case of the 1300 km^2 area shown in detail in Figure 3 (which covers two GFED grid cells from within the highlighted area of Figure 1f; which in total is covered by 192 GFED grid cells), all fifty of this area's MCD14 MODIS AF detections are considered very likely to be false alarms, and these are transformed by the SFB into 41 km^2 of burned area reported for these two cells alone in GFED4.1s. The total GFED4.1s burned area for the highlighted region of Figure 1f is 1017 km^2 in August 2015, most could possibly be coming from the SFB. To confirm these MODIS active fires as false, all MODIS AF pixels from the entire June to October period for eastern China were classified as likely 'true fires' or likely 'false alarms' using the AF false-alarm mask utilised by Reference [17], and were then evaluated for their impact on the GFED4.1s inventory at its native 0.25° resolution (Figure 4). Whilst large numbers of 'true' MODIS AF pixels were found in June and October 2015 within areas that the landcover

mask indicates as agricultural (Figure 7a from Reference [17]), substantial numbers of AF false alarms were found in August in the highlighted area of Figure 1f, confirming their responsibility for the anomalously boosted GFED4.1s BA, which is reported as 3093 km^2 (Figure 1f) compared to only 15 km^2 in GFED4 (Figure 1e). The monthly contribution of the 'boosted' BA from suspected true AF and false alarms was evaluated using these classified MODIS AF pixel counts. Figure 5a shows the amount of BA coming from the burned area mapped by the MODIS BA (MCD64A1) product (as used in GFED4), along with that added by the SFB applied in GFED4.1s. Figure 5b shows the breakdown of SFB BA contributed by suspected true AFs and false alarms. Apart from June and October, each month is dominated by false alarms rather than correct AF detections. The burned area reported for this region by GFED4.1s is thus dominated by active fire false alarms and the small fire boosting strategy, rather than by real burning. Total MODIS-measured BA for the region (as reported in GFED4) is 3550 km^2 for 2015, whilst the GFED4.1s boost adds a further 8589 km^2 in grid cells dominated by 'true' AF detections, and a further 14,353 km^2 in grid cells dominated by suspected 'false alarm' AF detections.

We conclude therefore that the use of the SFB in GFED4.1s appears to have correctly increased the magnitude of the MODIS-mapped BA during the key fire months of June and October (Figure 1), adjusting for some of the negative bias in burned area and fire emissions caused by the inability of the MCD64A1 product to confidently detect agricultural fire BA. For these months, the SFB has also significantly improved the agreement between the GFED4.1s BA record and the VIIRS-IM data, as can be seen in Figure 1. However, during August the GFED4.1s SFB strategy has introduced a significant false positive bias in the amount of burned area and thus in fire emissions, with the added burned area dominating the overall total measure of fire activity for this region and introducing a very significant BA (and thus fire emissions) signature during a month when fires are actually almost absent from the landscape.

3.2. Punjab, India

Burning in the Punjab region of India (Figure 2) is spread across a far smaller area than eastern China, and we therefore studied a single GFED 0.25° grid cell in detail, an area covering approximately 650 km^2 centred at 30.375° N, 74.875° E. Figure 6 shows that the MCD64A1 BA product reports negligible burning in October in this region (as therefore does GFED4), but reports dramatically increased burning in November (Figure 6a,b). This contrasts with the generally accepted situation that both October and November show significant agricultural burning in the Punjab region [15,20,25]. The boosted GFED4.1s shows slightly more BA in October than GFED4, though this still represents only 13% of the Oct-Nov total (Figure 6a). By contrast, the daily cumulative FRP data from the MODIS MCD14 and VIIRS-IM AF products show a generally linear trend over the October–November period (e.g., Figure 6c,d), agreeing with the general consensus that this region's fire activity is roughly comparable between the months of October and November. Thus, despite the MODIS AF product appearing to capture the temporal distribution of fire activity reasonably well for the months of October and November, these data have not led to a large enough BA bias correction when deployed in the SFB process used by Reference [11], and as implemented in GFED4.1s. To help understand this, ten Landsat 8 and Sentinel-2 scenes from the period were combined and used to map BA within the GFED grid cell analysed in Figure 6 at high spatial resolution. Mapping was done using the dNBR approach described in Section 2.3. The resulting BA timeseries (BA_dNBR; Figure 6e) starts to increase from the beginning of October, and shows a total cumulative burned area of around 200 km^2 by the end of that month, and over 550 km^2 by the end of November (equivalent to more than 80% of the GFED grid cell; see colour composites and BA_dNBR maps in Figure 7). The evolution of the BA_dNBR (Figure 6e) time series broadly matches the FRP timeseries recorded by MODIS and VIIRS-IM (Figure 6c,d), and the spatial distribution of fire activity indicated by these datasets are also broadly similar (Figure 7).

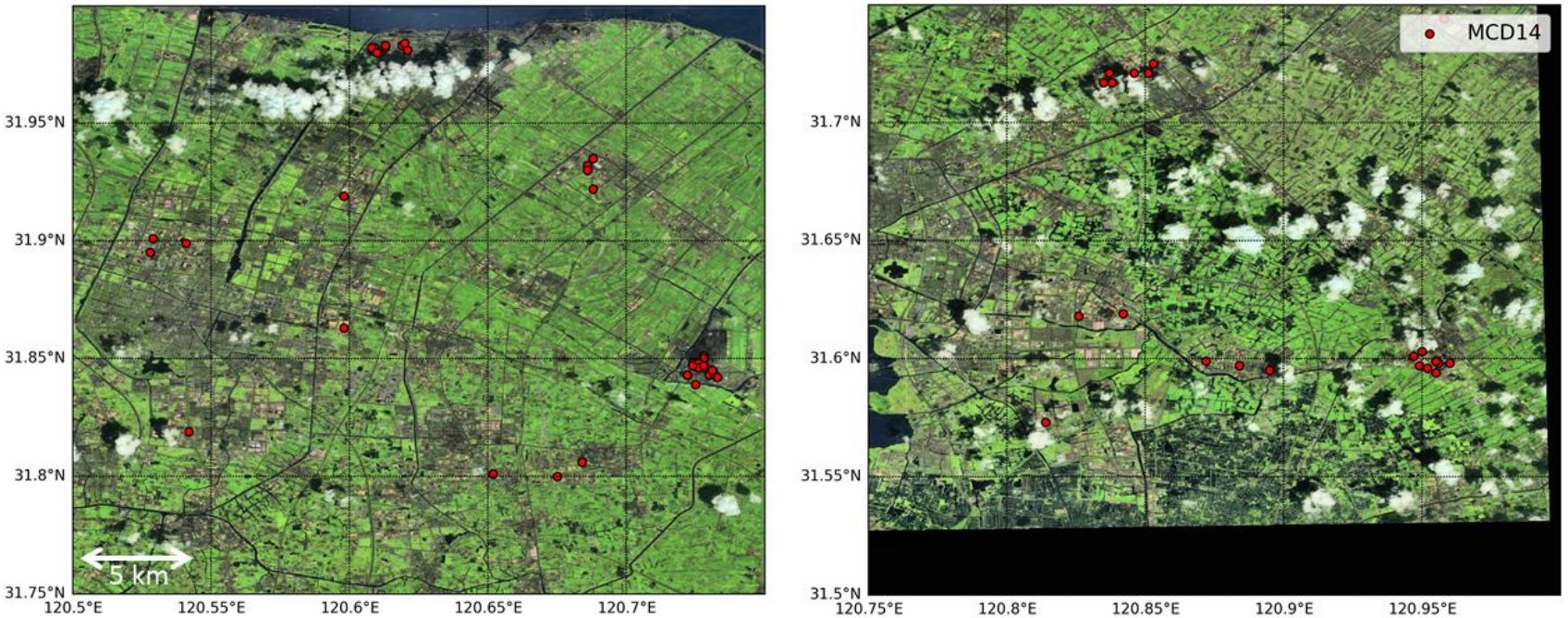

Figure 3. MODIS 1 km active fire (AF) detections produced using the algorithm described in [4] and displayed in red within two 0.25 deg × 0.25 deg areas (representing the areas of two GFED grid cells) in eastern China, overlaying Sentinel-2 true colour composites (centered at 31.875° N,120.625° E and 31.625° N,120.875° E respectively, retrieved on 22 August 2016). Every one of the MODIS AF detections can be seen to be located in an area where outdoor vegetation burning is unlikely to have occurred, for example in residential and industrial areas. None are on agricultural land, and it is therefore very likely that these AF detections are false alarms caused by manmade structures being warmer or more glint-inducing than their surroundings—as detailed in References [7,17]. Such effects mean AF detection algorithms are frequently subject to these types of false alarms in eastern China, and Reference [17] developed methods to mask these false alarms based on temporal persistence and landcover information. The MCD14 AF product does not apply such masking, so the false alarms remain, and their presence in areas not matched by MODIS burned area detections causes GFED4.1s to report significant burned area for these two grid cells (24 and 19 km^2, respectively). These large burned areas come from the application of the 'boosting' methodology of [11] which is used within GFEDv4.1s to 'boost' burned area undetected by the MODIS MCD64A1 BA product. This SFB method takes MODIS AF detections located at sites where there is matching MCD64A1 detected burned area and, once a calibration between AF count and BA size is developed, uses the AF's detected in areas where no MCD64A1 burned area detection occurs to estimate the 'undetected' BA from the presumed 'small fires' (see Figure 1f for locations of these cells and [11] for full details of the SFB methodology).

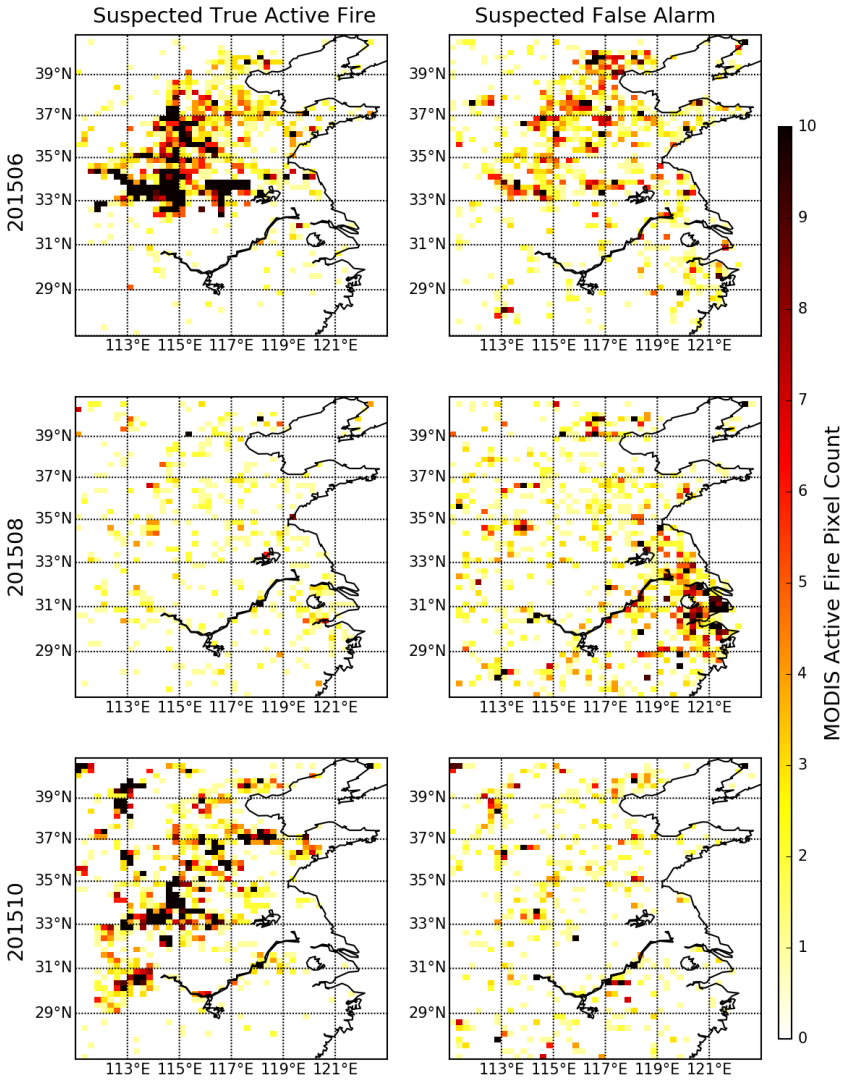

Figure 4. MODIS active fire (AF) pixel counts from MCD14 (0.25° grid cell resolution) in the eastern China region highlighted by the blue dashed box in Figure 1. AFs were classified via the landcover-based approach of Zhang et al. [17] as either suspected "true" active fire detections (left column), or false alarms (right column). The latter are identified by their occurrence in non-vegetated areas, such as urban regions (see [17] for more details). The 'true' and 'false alarm' AF counts are shown for June (upper row), August (middle row) and October 2015 (lower row), and false alarm AFs are clearly most apparent in August 2015 and in the region of eastern China highlighted in Figure 1f as showing a potentially suspicious region of very significantly 'boosted' GFED4.1s burned area.

Overall, these results indicate that to some extent, the SFB of GFED4.1s was able to correctly boost fire activity in October 2016 in the Punjab region compared to what was present in the original GFED4, but that the magnitude of this adjustment was insufficient to make up for the underestimation of agricultural fire BA present in the baseline MCD64A1 BA data, due to its limited ability to map the burns coming from the typically rather small agricultural fires. In November it appears that the MCD64A1 BA data provides far better detections than in October, possibly because the total cumulative burned area on the landscape has become very large by that stage.

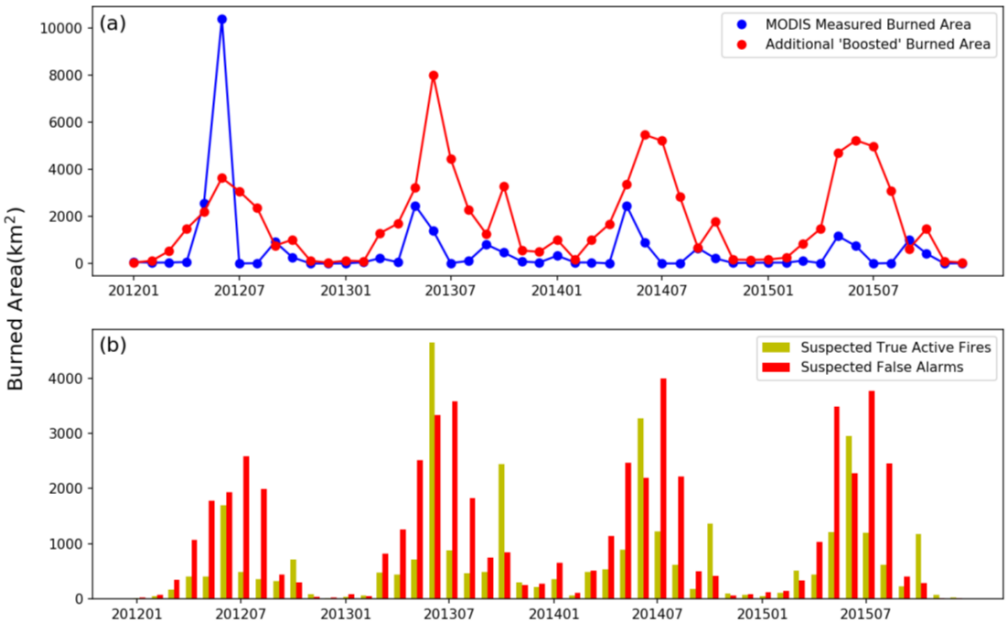

Figure 5. Monthly fire activity for 2012–2015 for eastern China (area shown in Figure 1). (**a**) GFED4-reported burned area (BA) (derived only from the MODIS MCD64A1 BA product), along with the additional BA reported in GFED4.1s that comes from the 'small fire boost' derived using the method reported in [11]). Most of the GFED4.1s BA comes from the SFB rather than actual MODIS BA mapping. (**b**) 'Boosted' BA data classified as either BA derived from suspected true active fire detections, or BA derived from suspected AF false alarms (classifiedusing landcover-based masking; see Figure 4).

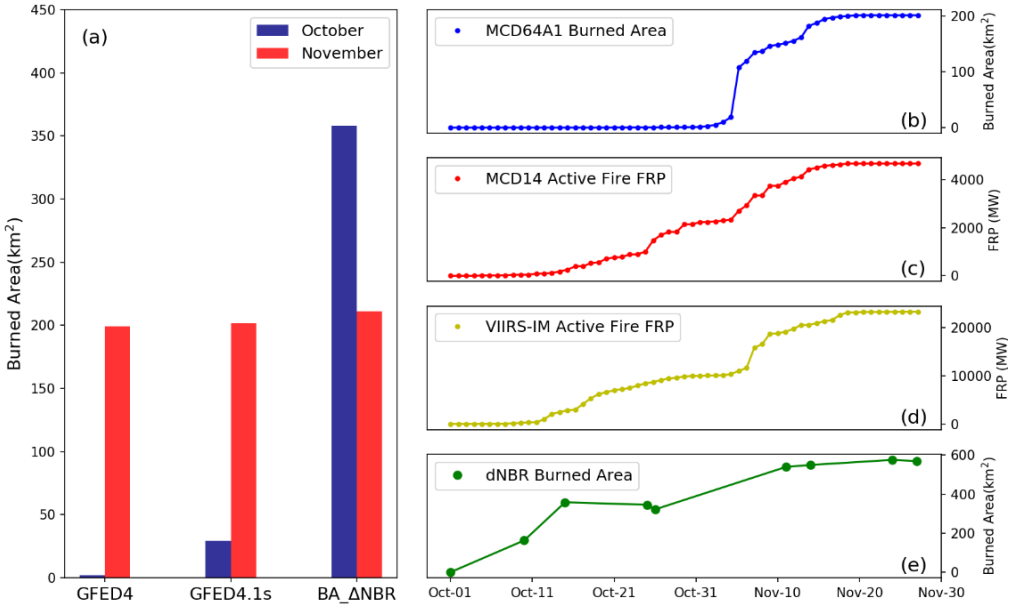

Figure 6. Total (**left column**) and cumulative time series (**right column**) of fire activity for October and November, 2016 for the 0.25° GFED grid cell located in the Punjab, north-western India (centred at 30.375° N, 74.875° E, shown spatially in Figure 7). (**a**) comparison of total BA in October (blue) and November (red) 2016 reported by GFED4 (based on MCD64A1) and GFED4.1s (based on MCD64A1 + the SFB of [11]), along with that derived from Landsat and Sentinel-2 dNBR-based BA mapping, and (right column) daily cumulative (**b**) MCD64A1 BA, (**c**) MCD14 FRP, (**d**) VIIRS-IM FRP, and (**e**) dNBR-derived BA from Landsat/Sentinel-2.

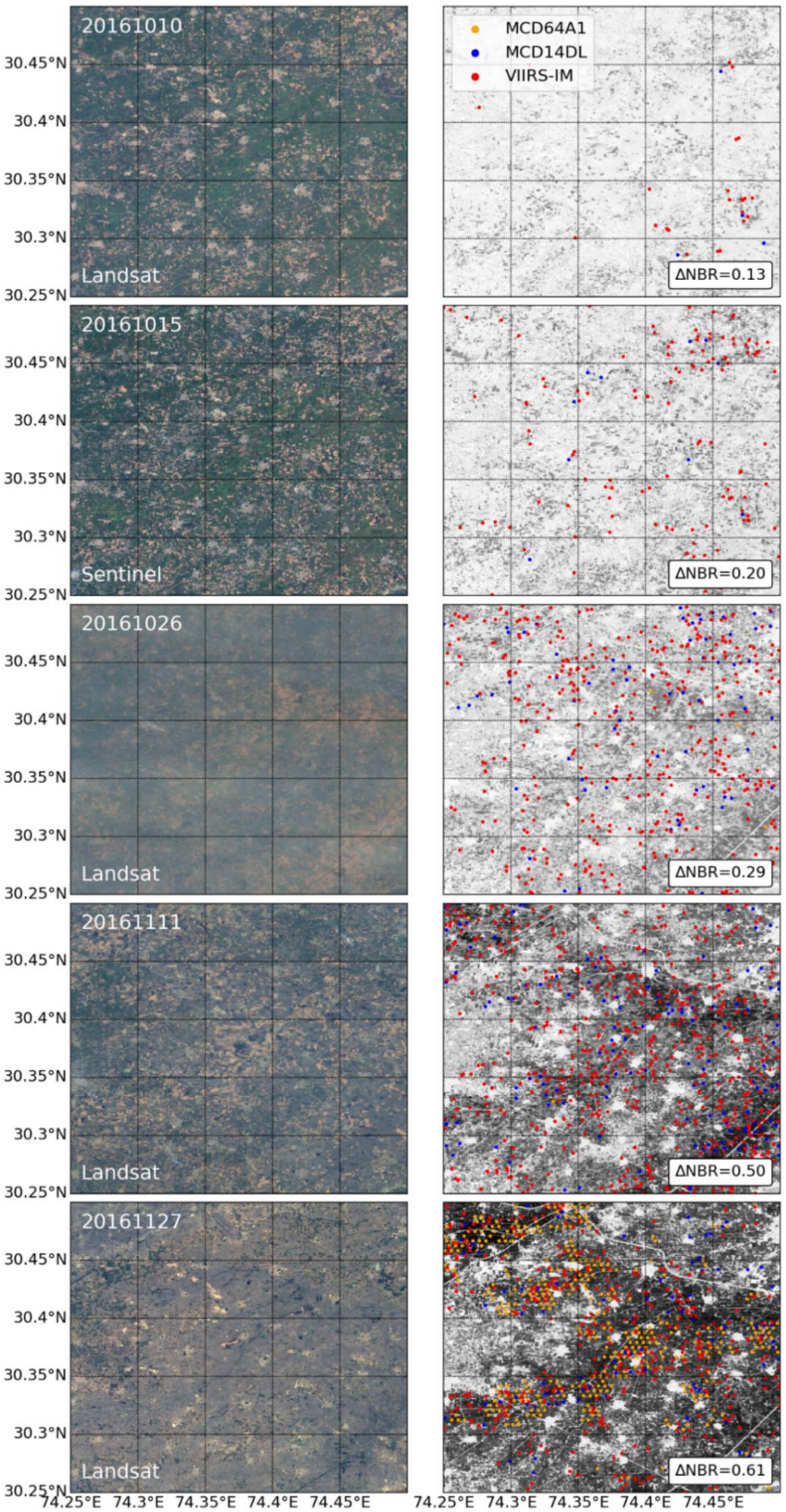

Figure 7. Detail of a 0.25° GFED grid cell centered at 30.375° N, 74.875° E, Punjab, India and imaged repeatedly over the October to November 2016 burning season. (**Left column**) true colour composites derived from Landsat/Sentinel-2 imagery, and (**right column**) ΔNBR map overlaid with burned area and AF detection data from MODIS and VIIRS collected during the interval between each Landsat/Sentinel-2 image. ΔNBR caption reports mean ΔNBR of the whole grid cell, and the amount of burned area present within the grid cell can be seen increasing from the 10 October 2016 to the 27 November 2016.

4. Underlying Issues with MCD64A1 and MCD14

Given the issues with the GFED-reported MODIS BA for agricultural regions identified in Section 3, further analysis of the underlying MODIS BA product (MCD64A1) was deemed necessary. This analysis was performed using comparisons between the MODIS-mapped BA and the MCD14 and VIIRS-IM AF products, and to Landsat/ Sentinel-2 imagery. The analysis was conducted for both the eastern China and Punjab study areas detailed in the previous Sections, and Figure 8 shows two cases where the MODIS MCD64A1 BA product clearly failed to identify fire affected areas.

Figure 8a–c gives an example of a relatively large (~50 km^2) fire in eastern China, covering almost half of the GFED 0.25° grid cell. Smoke and flames seen in the Landsat imagery of Figure 8b confirm the timing and location of the fire, but Figure 8d shows that the MODIS MCD64A1 product barely detected any BA here. By contrast, both MCD14 and VIIRS-IM AF products appear to delineate the fire affected area rather well, with the VIIRS-IM product's smaller pixel size enabling it to provide the most detailed representation of the shape and extent of the fire (Figure 8d), observed in the Landsat imagery (Figure 8c).

Figure 8e–h shows a similar analysis for a 0.25° region of the Punjab, but in this case the numerous fires present in the area are typically individually far smaller than those seen in the China example of Figure 8a–d. The MCD64A1 BA product consequently fails to detect many of the fires north of the river that bisects the grid cell, though it does appear to detect many that occur south of the river (Figure 8h). Figure 8h indicates that MCD14 also shows a similar performance, delivering an apparently reasonably record south of the river, but less so north of the river. These results indicate that both the MODIS BA and AF products fail to identify many of the fires in this particularly small-fire dominated landscape. By contrast, the smaller pixel area of the VIIRS-IM product has allowed it to detect far more AFs than does the MODIS MCD14 product (Figure 8h), and these AF detections agree well with the area of burning identified in the Landsat imagery timeseries (Figure 8e–g). This reflects the strong small fire sensitivity of the 375 m spatial resolution VIIRS I-Band when used with an appropriately optimised active fire detection algorithm, as reported by [7,17].

We also note some detection commission errors within the MCD64A1 BA data, which could relate to areas of harvesting incorrectly identified as burning by the MCD61A1 change detection algorithm (Figures 9 and 10). Figure 9 highlights a case in eastern China where the fire clusters detected by the MODIS MCD64A1 burned area product disagree with the AF detections of the MODIS MCD14 and VIIRS-IM products, and are also not co-located with any burn scars identifiable in the 30 m spatial resolution Landsat imagery. The MCD64A1-identified burned areas are dislocated in space (Figure 9a,b), and time (Figure 9c–e) relative to the active fire detections made with the other data sources. Most of the burned area was identified in the period 1–2 June by MCD64A1, whilst active fires only appear ten days later (11 June, both in the MODIS MCD14 and VIIRS-IM data. A possible explanation for this is that the MCD64A1 algorithm (which is primarily using changes in surface spectral reflectance ratios to identify areas of burning; see [25]) is actually identifying harvesting, since both processes applied in this environment are removing senescent surface vegetation and exposing soils beneath.

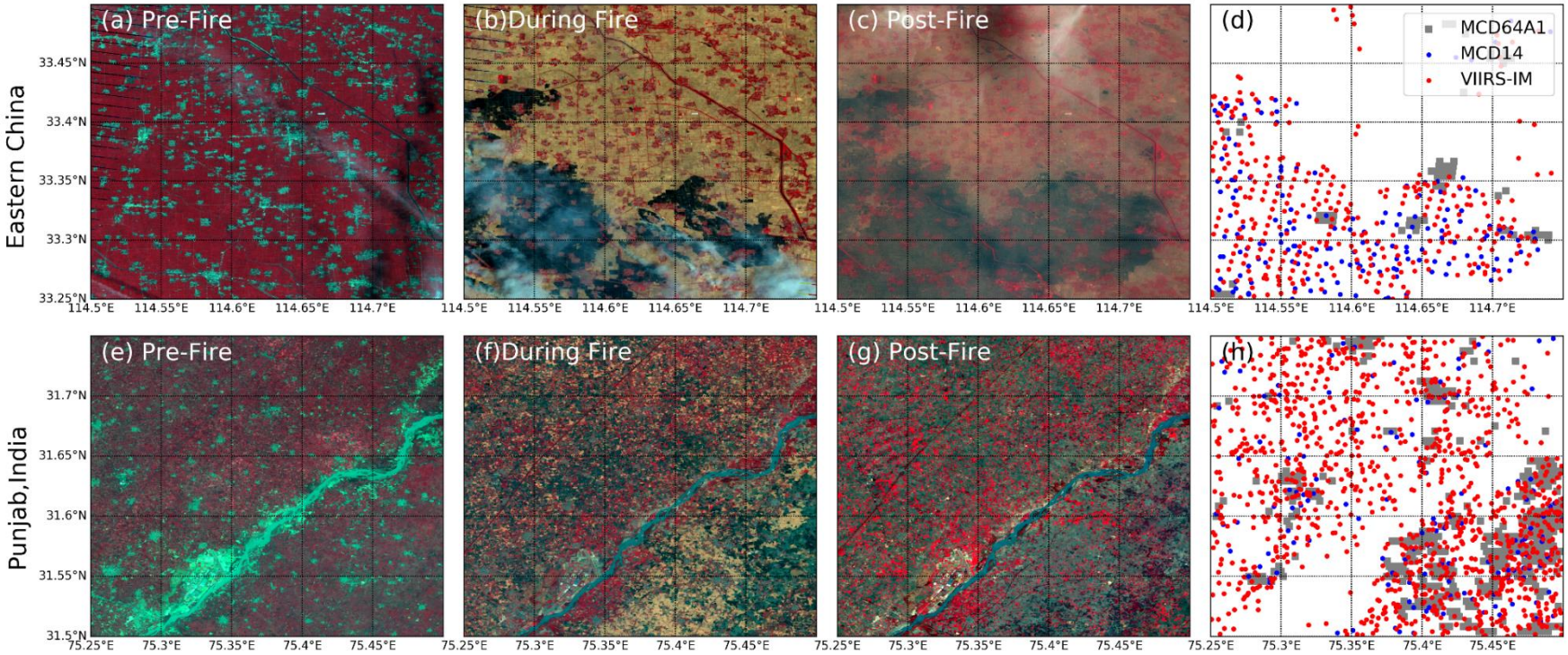

Figure 8. Fire-relevant data covering a 0.25° GFED grid cell in (**top row**) eastern China (centred at 33.375° N, 114.625° E), and (**bottom row**) the Punjab (northwestern India, centred at 31.625° N, 75.375° E). (**a**–**c**) show Landsat NIR false colour composites taken respectively before (24 April 2015), during (11 June 2015) and after (19 June 2015) the fire activity in eastern China, and (**e**–**g**) before (24 September 2016), during (26 October 2016) and after (27 November 2016) the fire activity in the Punjab, India. For comparison, (**d**,**h**) show the mapped fire activity respectively reported in these same two areas during the same period by the 500 m MODIS MCD64A1 burned area (BA) products, the 1 km MCD14 active fire (AF) product, and the 375 m VIIRS-IM AF product. Compared to the evidence from Landsat, eastern China appears to have large areas of burning missing in the MCD64A1 BA product, whereas in the Punjab the MCD64A1 product appears to do relatively well south of the river that bisects the grid cell from southwest to northeast, but less so north of the river where the small agricultural fires appear more fragmented in the Landsat imagery.

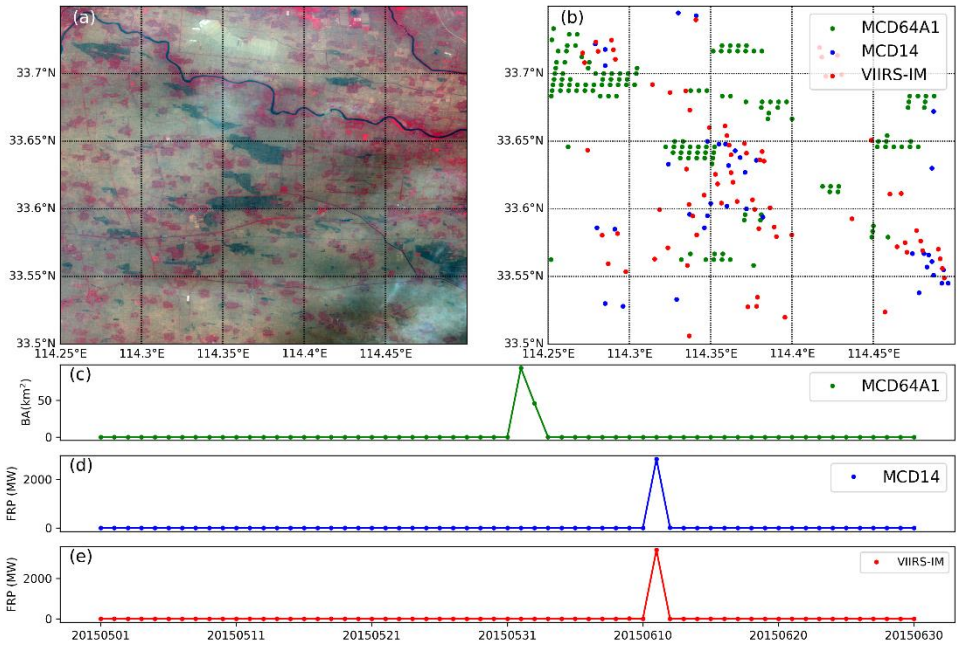

Figure 9. Fire activity within a 0.25° GFED grid cell centered at 33.625° N, 114.375° E in eastern China, May–June 2015? (**a**) Landsat-8 NIR false colour composite of 19 June 2015, after fire activity occurred in this grid cell. Recently burned areas appear dark in this rendition. (**b**) Spatial, and (**c**–**e**) temporal distribution of three fire products, MCD64A1 BA data, along with MCD14 and VIIRS-IM AF data. The spatial and temporal disagreement of MCD64A1 with MCD14, VIIRS-IM and the Landsat 8 imagery indicates that the burned area detected here by MCD64A1 seems likely to be caused by non-fire processes (e.g., crop harvesting) and is therefore represents an error of commission rather than true fire activity. When the fires do occur (as seen in the AF data) the MCD61A1 then fails to detect their 'real' burned area, resulting in a BA error of omission.

To investigate the scale of the temporal disagreement of the MCD64A1 burned area detections with two AF products shown in Figure 9, we further examined the 50 grids with the highest MCD64A1 detected BA from May to June 2012–2015 and compared the timing of the BA identification with that of the AF detections contained within the MODIS MCD14 and VIIRS-IM products (Figure 10). Almost all of the 200 cases examined from across 4-year shared the same temporal mismatch problem demonstrated in Figure 9. Taking the year 2014 as an example, both MCD14 and VIIRS-IM AF data suggest two fire peaks occurred around 10 June, whilst the BA data from MCD64A1 identified a peak around 31 May, ten days earlier than the active fire detections. The consistent temporal disagreement shown in Figures 9 and 10 suggests that the MCD64A1 BA data (and therefore the un-boosted GFED inventory measures which use it as their burned area metric) may be unsuited for studying the detail of fire activity and fire emissions in agricultural areas, where harvesting can be easily mistaken for burning by BA mapping algorithms using moderate spatial resolution imagery as input (e.g., MCD64A1). Therefore, not only is there a possibility that the MCD64A1 product is delivering a low-biased BA in such areas, but the timing of the burning is also sometimes erroneously shifted earlier in the season due to the burned area detection algorithm identifying harvesting as burning. The MODIS BA Product User Guide [25] in fact suggests that MCD64A1 burned area detections in croplands should generally be treated with a low degree of confidence, due to the inherent difficulty in mapping agricultural burning reliably with moderate spatial resolution datasets, including the potential confusion with processes such as harvesting. Active fire detection products can identify far smaller fires than the BA mapping products based on the same spatial resolution data, and also do not confuse fire detections with harvesting. Thus GFED4.1s deploys the MODIS AF products within the 'small fire boost' methodology [11] evaluated in Section 3 to attempt to correct for the low-biases

in MCD64A1 burned area. However, because MODIS' 1 km MCD14 AF detections suffer from many false alarms in eastern China during summer months such as August, some of the resulting very significant 'boosts' to burned area need to be treated with caution, as detailed in Section 3. We now also see that any problems resulting from the SFB's attempt at correcting for MCD61A1 errors of omission may actually in some cases be compounding errors caused by harvest-related MCD64A1 burned area mapping errors of commission, as depicted in Figures 8–10. However, it is the case that if it is assumed that the harvested fields will subsequently have their residues burned, the temporal error introduced by the mis-identification of harvesting as burning seen in Figure 9 may not be so important at a monthly temporal resolution, which is the default of GFED.

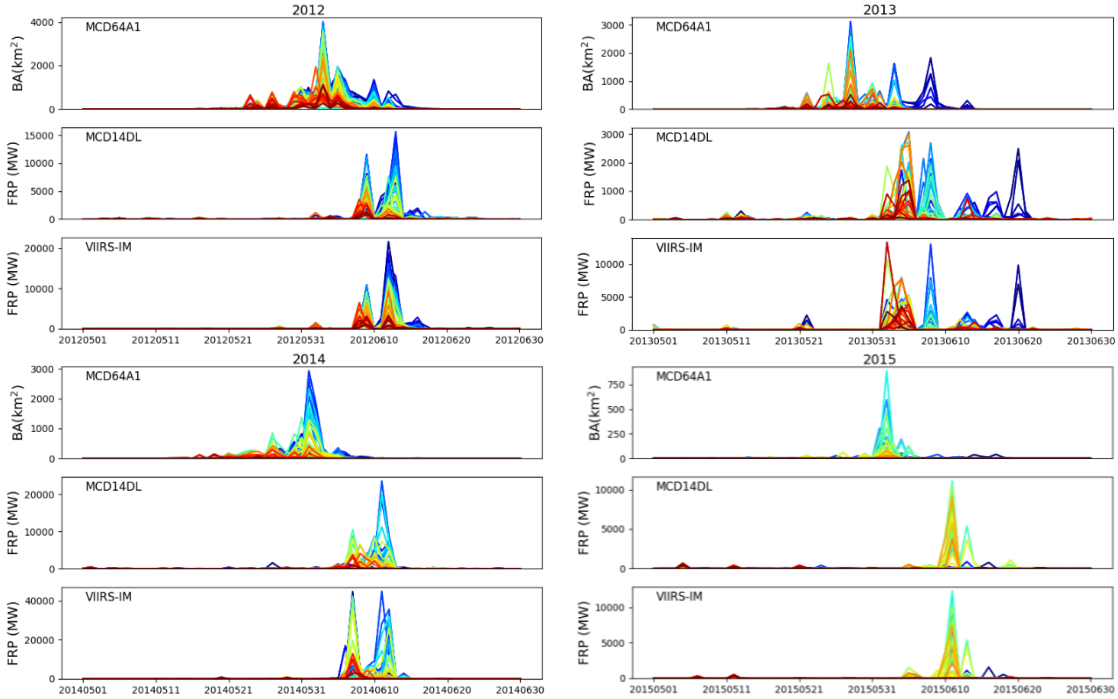

Figure 10. Time series of fire datasets for eastern China (region shown in Figure 1) during the summer burning season (May–June) from 2012–2015. The MODIS MCD64A1 product reports detected burned area (BA), and the MODIS MCD14DL and VIIRS-IM show retrieved fire radiative power (FRP) made at the locations of active fire (AF) detections. Colours represent different GFED grid cells within the region, and for clarity only those cells showing the fifty highest MCD64A1 burned area values are shown here. MCD64A1 reported burned area typically peaks 1 to 2 weeks before the AF products detect the peak in fire occurrence, suggesting that the BA product is identifying the initial harvesting of the crop rather than any subsequent burning of the crop residue left in the fields after harvest.

5. Summary and Conclusions

The most recent version of the widely used Global Fire Emissions Database (GFED4.1s) includes a version of the 'small fire boost' (SFB) methodology of [11] in an attempt to adjust for the low-biases in burned area (BA) reported by the MODIS MCD64A1 BA product. This upward adjustment in BA is particularly important in areas dominated by 'small fires', whose burned areas are difficult to map with the MODIS 500 m spatial resolution data that form the primary input to the MCD64A1 algorithm [10,11]. The GFED4.1s SFB approach is applied within each 0.25° GFED grid cell, and within each cell MODIS MCD14 active fire (AF) detections occurring outside of the burned areas mapped with MCD64A1 BA product are used to increase the reported burned area. The impact of this strategy is most significant in agricultural areas where crop residues are burned in the fields, as occurs for example across many parts of Asia [10]. Here the fire regime and fire emissions release is typically

dominated by very large numbers of individually small fires, whose smoke emissions have significant implications for local and regional air quality. By comparing information from GFED4.1s and the forerunner (unboosted) GFED4 inventories, along with the original MODIS MCD64A1 BA and MCD14 AF products and higher spatial resolution data available from VIIRS, Landsat and Sentinel-2, we have evaluated the performance and implications of the GFED4.1s SFB in the key agricultural burning regions of eastern China and the Punjab, north-western India.

In eastern China we find that during the peak two months of the fire season (June and October), the application of the SFB works reasonably well to correctly increase the BA estimated by the MODIS MCD64A1 product, and the 'boosted' BA in GFED4.1s appears therefore to better represent the timing and location of the agricultural fires occurring in these months compared to the 'unboosted' GFED4 MCD64A1 burned area alone. The GFED4.1s SFB thus appears to provide some definite benefit in these months for the agricultural fire emissions calculations. However, numerous false alarms present within the MODIS MCD14 AF product over industrial and urbanised areas of eastern China do introduce significant problems, most particularly in August when they manifest most strongly and act within the SFB methodology to introduce considerable additional 'boosted' BA into GFED4.1s during a period of the year when agricultural fires are in fact largely absent from eastern China. Our calculations suggest that more than half (around 54%) of the total dry matter fuel consumption reported by GFED4.1s in eastern China in the year examined here (2015) is a result of MODIS AF false alarms and the SFB approach, and thus the majority of the smoke emissions reported by GFED4.1s in this area of the world is false.

In the Punjab region, the October to November period is a major agricultural burning season [21,23], as seen in the AF datasets examined herein (Section 3). However, GFED4 only reports substantial fire activity in November, a consequence of the burned area omission errors in the underlying 500 m MCD64A1 BA product, which understandably often finds it difficult to identify small agricultural burns. The GFED4.1s SFB strategy correctly uses the MODIS AF detections to increase the reported BA for October, demonstrating some potential for the approach, but the magnitude of the BA increase is far too small to match the actual fire activity observed in higher spatial resolution BA data and AF time-series (Figure 6).

To investigate the underlying issues with the agricultural fire characterisations, we directly compared the MCD64A1 BA data with other remotely sensed fire datasets, and confirmed that the 500 m spatial resolution MODIS MCD64A1 product does indeed fail to detect much of the burning occurring in these agricultural regions, ranging from the individually small but highly numerous fires in the Punjab and to even relatively large (~50 km^2) burn patches in eastern China (hence the rational for the 'small fire boost' methodology developed by [11] and implemented in GFED4.1s). Furthermore, the MCD64A1 BA product also appears to sometimes mistakenly classify recently harvested areas as burning (Figures 9 and 10). These types of performance limitations in agricultural regions are known issues to some extent [25], and are one reason why AF products appear to provide significantly more reliable spatio-temporal patterns of fire activity in these 'small fire dominated' regions, especially those based on higher spatial resolution input data such as the 375 m VIIRS I-Band that can identify fires around 10× smaller than can the MODIS AF product [17]. The inability of the 1 km MODIS AF data to detect large numbers of the smallest agricultural fires in the Punjab region appears to be the cause of the GFED SFB strategy failing to deliver the magnitude of BA increase needed in October 2016 for example (Figure 6a). Nevertheless, the SFB approach does increase the reported BA in this month, and so shows some potential for improving biomass burning estimates in such small-fire dominated regions. However, this ability is limited in many ways, and beyond not providing the correct magnitude of bias correction, the SFB strategy risks introducing into the GFED inventory incorrect representations of fire activity at certain times of the year, as we have found has occurred in eastern China. The varied performance of the GFED4.1s SFB found in eastern China and the Punjab region, which represent some of the most significant areas of agricultural burning worldwide, implies that the GFED4.1s cannot necessarily be relied upon to deliver the correct timing, spatial extent and magnitude of fire activity in areas dominated by agricultural burning (and possibly

other types of 'small fire' dominated' biome). Therefore, we recommend that GFED4.1s users examine the contribution of the 'boosted' BA/emissions to the total BA/emissions prior to the use of this important fire emissions database, especially in areas that might be expected to be dominated by smaller fires. These data fields are present in GFED4.1s and enable users to identify where the SFB has had the greatest impact on the reported fire emissions. Future work to enhance the performance of this type of burned-area based fire emissions inventory in small fire dominated areas, such as agricultural regions, should very likely focus on the introduction of higher spatial resolution BA data, such as that derived from Landsat or Sentinel-2. If active fire data are used in future implementations of the GFED small fire boosting strategy, then consideration should be given to improving its performance and representativeness by using higher spatial resolution sources such as the VIIRS I-Band, and to employing strategies to identify and pre-mask active fire false alarms in regions where these are known to dominate [7,17].

Author Contributions: T.Z. and M.J.W. designed the experiments; T.Z. performed the experiments; T.Z. and W.X. analyzed the data; T.Z., M.J.W. and M.C.d.J. wrote and edited the paper.

Acknowledgments: VIIRS-IM AF product processing and storage was conducted using the UK's JASMIN super-data-cluster system, managed by UK STFC's Centre for Environmental Data Analysis (CEDA). We gratefully acknowledge the King's China Award and King's Graduate School who funded T. Zhang. This study was supported primarily by funding from the Natural Environment Research Council (NERC) of the UK (NCEO award PR140015 and NERC Research Grant NE/M017729/1).

Conflicts of Interest: The authors declare no conflict of interest.

References

1. Seiler, W.; Crutzen, P.J. Estimates of gross and net fluxes of carbon between the biosphere and the atmosphere from biomass burning. *Clim. Chang.* **1980**, *2*, 207–247. [CrossRef]
2. Van der Werf, G.R.; Randerson, J.T.; Giglio, L.; Collatz, G.J.; Mu, M.; Kasibhatla, P.S.; Morton, D.C.; DeFries, R.S.; Jin, Y.V.; van Leeuwen, T.T. Global fire emissions and the contribution of deforestation, savanna, forest, agricultural, and peat fires (1997–2009). *Atmos. Chem. Phys.* **2010**, *10*, 11707–11735. [CrossRef]
3. Giglio, L.; Randerson, J.T.; Werf, G.R. Analysis of daily, monthly, and annual burned area using the fourth-generation global fire emissions database (GFED4). *J. Geophys. Res. Biogeosci.* **2013**, *118*, 317–328. [CrossRef]
4. Giglio, L.; Descloitres, J.; Justice, C.O.; Kaufman, Y.J. An enhanced contextual fire detection algorithm for MODIS. *Remote Sens. Environ.* **2003**, *87*, 273–282. [CrossRef]
5. Giglio, L.; Van der Werf, G.R.; Randerson, J.T.; Collatz, G.J.; Kasibhatla, P. Global estimation of burned area using MODIS active fire observations. *Atmos. Chem. Phys.* **2006**, *6*, 957–974. [CrossRef]
6. Giglio, L.; Loboda, T.; Roy, D.P.; Quayle, B.; Justice, C.O. An active-fire based burned area mapping algorithm for the MODIS sensor. *Remote Sens. Environ.* **2009**, *113*, 408–420. [CrossRef]
7. Schroeder, W.; Oliva, P.; Giglio, L.; Csiszar, I.A. The New VIIRS 375 m active fire detection data product: Algorithm description and initial assessment. *Remote Sens. Environ.* **2014**, *143*, 85–96. [CrossRef]
8. Wooster, M.J.; Roberts, G.; Perry, G.L.W.; Kaufman, Y.J. Retrieval of biomass combustion rates and totals from fire radiative power observations: FRP derivation and calibration relationships between biomass consumption and fire radiative energy release. *J. Geophys. Res. Atmos.* **2005**, *110*. [CrossRef]
9. Roy, D.P.; Boschetti, L.; Justice, C.O.; Ju, J. The collection 5 MODIS burned area product—Global evaluation by comparison with the MODIS active fire product. *Remote Sens. Environ.* **2008**, *112*, 3690–3707. [CrossRef]
10. Van der Werf, G.R.; Randerson, J.T.; Giglio, L.; van Leeuwen, T.T.; Chen, Y.; Rogers, B.M.; Mu, M.; van Marle, M.J.; Morton, D.C.; Collatz, G.J.; et al. Global fire emissions estimates during 1997–2016. *Earth Syst. Sci. Data* **2017**, *9*, 697. [CrossRef]
11. Randerson, J.T.; Chen, Y.; Werf, G.R.; Rogers, B.M.; Morton, D.C. Global burned area and biomass burning emissions from small fires. *J. Geophys. Res. Biogeosci.* **2012**, *117*. [CrossRef]
12. Chan, C.K.; Yao, X. Air pollution in mega cities in China. *Atmos. Environ.* **2008**, *42*, 1–42. [CrossRef]
13. Chen, J.; Li, C.; Ristovski, Z.; Milic, A.; Gu, Y.; Islam, M.S.; Wang, S.; Hao, J.; Zhang, H.; He, C.; et al. A review of biomass burning: Emissions and impacts on air quality, health and climate in China. *Sci. Total Environ.* **2017**, *579*, 1000–1034. [CrossRef] [PubMed]

14. Granier, C.; Bessagnet, B.; Bond, T.; D'Angiola, A.; van Der Gon, H.D.; Frost, G.J.; Heil, A.; Kaiser, J.W.; Kinne, S.; Klimont, Z.; et al. Evolution of anthropogenic and biomass burning emissions of air pollutants at global and regional scales during the 1980–2010 period. *Clim. Chang.* **2011**, *109*, 163. [CrossRef]
15. Sharma, A.R.; Kharol, S.K.; Badarinath, K.V.S.; Singh, D. Impact of agriculture crop residue burning on atmospheric aerosol loading—a study over Punjab State, India. *Ann. Geophys.* **2010**, *28*, 367. [CrossRef]
16. Zhang, T.; Wooster, M.J.; Green, D.C.; Main, B. New field-based agricultural biomass burning trace gas, PM2. 5, and black carbon emission ratios and factors measured in situ at crop residue fires in Eastern China. *Atmos. Environ.* **2015**, *121*, 22–34. [CrossRef]
17. Zhang, T.; Wooster, M.J.; Xu, W. Approaches for synergistically exploiting VIIRS I-and M-Band data in regional active fire detection and FRP assessment: A demonstration with respect to agricultural residue burning in Eastern China. *Remote Sens. Environ.* **2017**, *198*, 407–424. [CrossRef]
18. National Bureau of Statistics of China (NBSC). *China Statistical Yearbook 2012*; National Bureau of Statistics of China (NBSC): Beijing, China, 2012.
19. Streets, D.G.; Bond, T.C.; Carmichael, G.R.; Fernandes, S.D.; Fu, Q.; He, D.; Klimont, Z.; Nelson, S.M.; Tsai, N.Y.; Wang, M.Q.; et al. An inventory of gaseous and primary aerosol emissions in Asia in the year 2000. *J. Geophys. Res. Atmos.* **2003**, *108*. [CrossRef]
20. Vadrevu, K.P.; Ellicott, E.; Badarinath, K.V.S.; Vermote, E. MODIS derived fire characteristics and aerosol optical depth variations during the agricultural residue burning season, north India. *Environ. Pollut.* **2011**, *159*, 1560–1569. [CrossRef] [PubMed]
21. Jain, N.; Bhatia, A.; Pathak, H. Emission of air pollutants from crop residue burning in India. *Aerosol Air Qual. Res.* **2014**, *14*, 422–430. [CrossRef]
22. French, N.H.F.; Kasischke, E.S.; Hall, R.J.; Murphy, K.A.; Verbyla, D.L.; Hoy, E.E.; Allen, J.L. Using Landsat data to assess fire and burn severity in North American boreal forest region: An overview and summary of results. *Int. J. Wildl. Fire* **2008**, *17*, 443–462. [CrossRef]
23. Mandanici, E.; Bitelli, G. Preliminary Comparison of Sentinel-2 and Landsat 8 Imagery for a Combined Use. *Remote Sens.* **2016**, *8*, 1014. [CrossRef]
24. Huang, X.; Li, M.; Li, J.; Song, Y. A high-resolution emission inventory of crop burning in fields in China based on MODIS Thermal Anomalies/Fire products. *Atmos. Environ.* **2012**, *50*, 9–15. [CrossRef]
25. Giglio, L.; Boschetti, L.; Roy, D.; Hoffmann, A.A.; Humber, M. Collection 6 MODIS Burned Area Product User's Guide Version 1.0. 2016. Available online: http://modis-fire.umd.edu/pages/manuals.php (accessed on 20 May 2018).